Journal Pre-proof

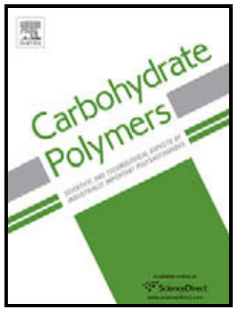

Novel halochromic cellulose nanowhiskers from rice straw: Visual detection of urea

Tawfik A. Khattab, Moustafa M.G. Fouda, Mohamed Rehan, Mohammad K. Okla, Saudi A. Alamri, Ibrahim A. Alaraidh, Abdullah A. AL-ghamdi, Walid H. Soufan, Eslam M. Abdelsalam, Ahmed A. Allam

PII: S0144-8617(19)31408-0

DOI: https://doi.org/10.1016/j.carbpol.2019.115740

Reference: CARP 115740

To appear in: *Carbohydrate Polymers*

Received Date: 15 October 2019

Revised Date: 11 December 2019

Accepted Date: 12 December 2019

Please cite this article as: Khattab TA, Fouda MMG, Rehan M, Okla MK, Alamri SA, Alaraidh IA, AL-ghamdi AA, Soufan WH, Abdelsalam EM, Allam AA, Novel halochromic cellulose nanowhiskers from rice straw: Visual detection of urea, *Carbohydrate Polymers* (2019), doi: https://doi.org/10.1016/j.carbpol.2019.115740

Novel halochromic cellulose nanowhiskers from rice straw: Visual detection of urea

Tawfik A. Khattab[1,*], Moustafa M. G. Fouda[2], Mohamed Rehan[2,*] rehan_nrc@yahoo.com**, Mohammad K. Okla[3], Saudi A. Alamri[3], Ibrahim A. Alaraidh[3], Abdullah A. AL-ghamdi[3], Walid H. Soufan[4], Eslam M. Abdelsalam[3], Ahmed A. Allam[5]**

[1] Dyeing, Printing and Auxiliaries Department, Textile Industries Research Division, National Research Centre, 33 El-Buhouth Street, Dokki, Cairo 12622, Egypt.
[2] Pretreatment and Finishing of Cellulosic-based Fibers Department, Textile Industries Research Division, National Research Centre, 33 El-Buhouth Street, Dokki, Cairo 12622, Egypt.
[3] Department of Biology, College of Science, King Saud University, Riyadh, Saudi Arabia.
[4] Plant Production Department, College of Food and Agriculture Sciences, King Saud University, Riyadh, Saudi Arabia.
[5] Department of Zoology, Faculty of Science, Beni-Suef University, Beni-Suef, 65211 Egypt.

[*]**Corresponding author:** Dr. Mohamed Rehan

Highlights

- Facile development of chromogenic biosensor for determination of urea.
- Cellulose nanowhiskers were loaded with a spectroscopic probe and urease enzyme.
- Detection limit was in the concentration range 50-1100 ppm.
- Response time of about 5-10 minutes.
- Color shift from light yellow to pink was monitored upon detection of urea.

Abstract

Colorimetric nanocomposite film sensor was fabricated by incorporating TCFH spectroscopic probe into cellulose nanowhiskers (CNW)/Urease enzyme matrix. CNW-TCFH can be used as disposable molecular biosensor in which CNW is the probe carrier comprising high surface area-to-volume ratio, urease is the catalyst and TCFH is the molecular probe. Tricyanofuran-hydrazone (TCFH) spectroscopic probe was prepared. UV-Vis absorption spectra demonstrated solvatochromic behavior and a reversible color change of the tricyanofuran-hydrazone probe solution in acetone under acid/base conditions. CNW were reinforced with sodium alginate biopolymer to introduce biocomposite film. This CNW-TCFH film biosensor responds through visible color shift from light yellow to pink when exposed to urea in aqueous media. The morphology properties of CNW and CNW-TCFH films were examined by different tools. The photophysical properties of the prepared TCFH probe, including solvatochromism and pH sensory, were also studied.

Keywords: Rice Straw; Cellulose Nanowhiskers; Urease; Halochromism; Urea; Biosensor.

1. Introduction

Chronic kidney failure is a common worldwide disease that may lead to high risk of death as a result of the considerable increments in the releasing levels of the body metabolic wastes into blood, such as urea that is normally discharged by kidney (D'Apolito et al., 2015; Jha et al., 2013; Webster, Nagler, Morton, & Masson, 2017). The total content of blood urea in a patient with a chronic kidney failure (50-70mM) may increase up to 10 times its magnitude in normal individuals (2.5-7.1mM). Thus, urea levels in both urine and blood are a significant diagnostic tool for kidney failure stages (Coresh, Astor, Greene, Eknoyan, & Levey, 2003; Levey et al., 2005; Testani, Cappola, Brensinger, Shannon, & Kimmel, 2011). There are various techniques have been provided for determination of urea, such as the electrochemistry-based tools and gas chromatography isotope dilution mass spectrometry (Palmas, Mussap, & Fattuoni, 2018; Sha, Komori, & Badhulika, 2017). However, they are sophisticated techniques characterized by low sensitivity and specificity, high cost, and time consuming (Y.-L. Liu et al., 2018). Thus, there has been increasing demands for the simple development of easy

to use and low cost diagnostic tools for clinical purposes. The ideal design of those sensing devices typically applies nanomaterials bearing active sites able to identify the existence of a specific analyte by fluorescence and/or colorimetric methods (Khattab, Dacrory, Abou-Yousef, & Kamel, 2019b; Khattab, Fouda, et al., 2019; J. Liu & Lu, 2006; Zheng et al., 2013). However, fluorescence-based detection tools generally undergo paramagnetic fluorescence quench, particularly in biofluids, upon binding with metal ions. Additionally, their application in aqueous medium is restricted as a result of their low solubility (Khattab, Kassem, Adel, & Kamel, 2019). Moreover, they necessitate sophisticated sensor assembly and expensive purification for urea detection (Carter, Young, & Palmer, 2014; Valeur & Leray, 2000). In this context, a colorimetric diagnostic tool composed of a combination of host paper sheet, nanomaterial-based carrier and active detection sites, is more promising (Khattab, Fouda, et al., 2018). Such detection system is characterized by simplicity of preparation, low cost, higher sensitivity and specificity, and easy real-time on-site naked-eye detection. Additionally, it requires uncomplicated instruments and less labor (Khattab, Dacrory, Abou-Yousef, & Kamel, 2019a; Schoolaert, Hoogenboom, & De Clerck, 2017). Nanomaterials have been an ever growing field toward a variety of applications such as medical diagnostics, drug delivery, nanomedicines, agriculture, foodstuffs processing, and ecological monitoring (R. Zhang & Chen, 2017). There are a wide range of nanomaterials that have been modulated to introduce sensing capabilities, however, cellulose nanowhiskers (CNW) has received a little consideration in this regard (Meng, Stolz, Mendecki, & Mirica, 2019; Penner, 2017). CNW possess several favorable characteristics such as abundance, renewability, low cost, low density, large and modifiable surface area, biocompatibility and biodegradability and they have been employed broadly to reinforce polymer composites (Kim et al., 2015). Due to the above characteristics, CNW demonstrated vast potential in different engineering applications such as optical and electronic devices, paper making, coating additives, food packaging, cosmetics, composite materials and molecular biology (Hoeng, Denneulin, & Bras, 2016; Serpa et al., 2016).

Biosensors have been used in various applications, such as medical and foodstuff industries, pharmaceuticals, and environmental monitoring (Fan et al., 2008; Länge, Rapp, & Rapp, 2008; Shao et al., 2010; Wang, 2005). In comparison to other analytical

techniques, enzyme-based detection tools are characterized by several advantages, such as low cost, and high sensitivity and specificity (Kharitonov, Zayats, Lichtenstein, Katz, & Willner, 2000). Among a variety of substrates that have been used for carrying enzymes, cellulose and its derivatives have been considered as one of the typical matrices because they are characterized by renewability, biodegradability and biocompatibility as well as being low cost and non-toxic (Cruys-Bagger et al., 2012; Rabinovich et al., 2007). There are two well-known enzymes, trypsin and α-chymotrypsin, were incorporated via adsorption on a microcrystalline cellulose matrix; however, this method is reversible and consequently, not scalable (Kumari, Chauhan, Ahn, & Reddy, 2016; Stoytcheva, Zlatev, Cosnier, Arredondo, & Valdez, 2013; Zaccheo & Crooks, 2011). One of the major problems in preparing efficient enzyme-based sensors is to guarantee that the incorporated enzyme can be maintained active over a period of time (Grishkewich, Mohammed, Tang, & Tam, 2017). Immobilization of urease enzyme trapped in a photopolymer onto a transducer surface can provide an effective biosensor for urea determination over a wide concentration range (0.5-15 mM) with rapid response time (1-2 min) (Duong & Rhee, 2015; Konda R Kunduru, Kutcherlapati, Arunbabu, & Jana, 2017). Enzymes can be attached to cellulose nanowhiskers via covalent bond, salt bridge or via physical inclusion complex. The surface characteristics of cellulose nanowhiskers afford a biocompatible matrix for this selective activity to take place (Dong et al., 2016; Lin, Gèze, Wouessidjewe, Huang, & Dufresne, 2016). Glucose oxidase incorporated onto a composite of cellulose nanocrystals and gold nanoparticles linked via thiols of polyethylenimine was able to function as a colorimetric biosensor giving different levels of activity depending on the number of thiol linkers (Su, Jiang, & Wang, 2015). Urease enzyme covalently incorporated onto modified cellulose fibers and activated by glutaraldehyde, considerably enhanced the sensor stability against temperature (Virgen-Ortíz et al., 2017). The simultaneous integration of several components in an assembly process of a sensing device has been a challenge in the fabrication of a comprehensive diagnostic tool. To defeat this difficulty, the co-immobilization of those targeted components in an inactive polymer matrix, mainly poly(acrylamide), have been applied via micro-emulsion polymerization (Cai, Xie, Zhang, Tang, & Tang, 2018; Konda Reddy Kunduru, Basu, Abtew, Tsach, & Domb, 2017). This tool is effective as an optical

detection system, but it is as well a tough process for the encapsulation of both a peptide and an enzyme because of the organic solvents involved in the process of capsule formation. Alginate films do not have this drawback as it can be applied in an aqueous environment at moderate circumstances. The active layer can be created via cross-linking of alginate directly by replacing monovalent sodium cations with divalent calcium cations (Desai, Koshy, Hilderbrand, Mooney, & Joshi, 2015; Palomo et al., 2016; M. Zhang et al., 2017).

Herein, we report the immobilization of urease onto cellulose nanowhiskers and its application as functional fillers into sodium alginate biocomposite layer (urea biosensor). We present pH colorimetric biosensor from cellulose nanowhiskers, efficiently turning them into chromic nanowhiskers composite film, demonstrating the value of this sensing nanomaterial. In this study, cellulose nanowhiskers (CNW) is prepared from cellulosic rice straw by acid hydrolysis to be used as a nanofiller able to carry a sensor dye and urease enzyme in a sodium alginate film loaded onto cellulose paper strips for practical application. Chromogenic thin film for real-time naked-eye colorimetric monitoring of aqueous urea is reported. Such urea biosensor is helpful for *on-site* detection of urea. Cellulose nanowhiskers were prepared from Rice straw wastes via strong acid hydrolysis process. A simple and reversible TCFH spectroscopic probe that is composed of tricyanofuran (TCF) acceptor and hydrazone (H) donor moieties is prepared to function as optical molecular-switching probe. Tricyanofuran-hydrazone (TCFH) spectroscopic probe was prepared via azo coupling reaction of tricyanofuran (TCF) heterocyclic coupler bearing active methyl group and diazonium chloride salt of 4-formylaniline. This tricyanofuran-hydrazone (TCFH) spectroscopic probe demonstrated a reversible color change due to pH variation was a result of charge delocalization on a generated hydrazone-anion leading to a quinoid-type molecular switch. TCFH is included in the alginate/CNW blended film as a pH indicator. Urease has been employed in combination with urea to produce ammonia as a reaction product. The influence of TCFH content on the photophysical properties of the produced films was studied. The nanocomposite film containing 1.5 wt % TCFH possessed the best sensing properties. The crosslinked calcium alginate stabilize the CNW film on the cellulose paper sheet forming an outer layer over urease enzyme and TCFH active sites, which interprets the urease/urea

interaction into a visible color shift detected by a signal on a paper strip. The high surface area of the nanowhiskers and their porous architecture afford higher adsorption on the surface of the miniaturized cellulosic nanowhiskers and better diffusion into the sensor bulk. The drop-casting process is employed to produce a tunable solid-state sensing film, which can function like a test paper. Transmission electron microscope, scanning electron microscopy (SEM), Fourier-transform infrared (FTIR) spectrometer and energy-dispersive X-ray spectroscopy (EDS) were employed to examine the properties of the created nanoscale morphology. Due to the enlarged surface area, the miniaturized sensor film exhibited high sensitivity upon exposing to ammonia released from the reaction of urea and urease enzyme. The photophysical properties, detection limit and reversibility were described. In addition, the response of TCFH to solvents of various polarities (solvatochromism) and different pH values (halochromism) in homogenous solution were also examined.

2. Experimental Details

2.1. Methods and instruments

Melting temperature (°C) was recorded uncorrected using Stuart-SMP30. Fourier-transform infrared (FTIR) spectra were explored in the range of 4000-400 cm^{-1} and at spectra resolution of 4.0 cm^{-1} employing Nexus 670 spectrophotometer (Nicolet, USA). UV/Vis absorption spectra of TCFH in different solvents and at different pH values were investigated under ambient conditions (25 °C) using UNICAM/UV-visible 300. NMR spectroscopy was explored employing BRUKER/AVANCE/400 at 400 MHz with chemical shifting in ppm relative to tetramethylsilane (TMS) under ambient conditions (25 °C). The morphological characteristics of nanocellulose were explored by Quanta FEG 250 scanning electron microscope (SEM) operating at 30 kV. SEM was connected to Energy-Dispersive X-ray Spectroscope (TEAM-EDX Model) which was employed to study the elemental content at an operational distance of 21mm and an acceleration voltage of 20kV. The diameter of the nanowhiskers was recorded by SEM Image J software. Cellulose nanowhiskers were also characterized by transmission electron microscope (TEM) using JEOL 1230 (Tokyo, Japan) at an accelerating voltage of 100KV. A drop of nanocellulose suspension was applied on a copper grid comprising a carbon film. The pH value was reported using AD-11 ADWA digital pH meter.

2.2. Materials and reagents

Urease enzyme (Jack bean, Canavalia ensiformis) was obtained from Fluka. Solvents were purchased from Aldrich and Fluka for both spectroscopic measurements (spectroscopic grade) and synthesis processes. Both calcium chloride and sodium alginate were obtained from Sigma-Aldrich. Whatman cellulose-based filter paper model with off-white color, pore size (11 μm), diameter (240 mm), thickness (180 μm), and basis weight (87 g/m^2); were purchased from Sigma-Aldrich. Double distilled water was applied in all experiments. Tricyanofuran **1** was prepared according to literature procedure (Abou-Yousef, Khattab, Youssef, Al-Balakocy, & Kamel, 2017; Khattab et al., 2017; Khattab, Tiu, Adas, Bunge, & Advincula, 2016) starting from 3-hydroxy-3-methyl-2-butanone and malononitrile (1:2 molar ratio) in sodium ethoxide solution to afford an off-white crystalline solid (yield 55%); mp 200-202˚C; ^{1}H NMR (400 MHz, $CDCl_3$) δ (ppm): 2.35 (s, 3H), 1.63 (s, 6H); ^{13}C NMR (400 MHz, DMSO-d_6), δ (ppm): 185.61, 177.08, 112.03, 111.26, 109.79, 103.53, 101.18, 54.68, 23.11, 14.13. 4-Formylaniline was prepared according to previously reported procedure starting from 4-nitrobenzaldehyde in presence of $SnCl_2 \cdot 2H_2O$ as a catalyst and using ethanol as a solvent (Abou-Yousef et al., 2017; Khattab et al., 2017; Khattab et al., 2016). 4-formylaniline was obtained as a yellow oil in a relatively high yield (82%); ^{1}H NMR (400 MHz, $CDCl_3$) δ (ppm): 9.76 (s, 1H), 7.70 (d, 2H), 6.74 (d, 2H), 4.10 (s broad, 2H). Tricyanofuran-hydrazone **4** was synthesized via an azo coupling reaction among the diazonium chloride salt of 4-aminobenzaldehyde **2** and TCF coupler **1** to give an orange solid powder with a relatively high yield (85%); mp 227-228˚C; ^{1}H NMR (400 MHz, $CDCl_3$) δ (ppm): 12.89 (s broad, 1H, NH), 9.91 (s, 1H, CHO), 8.25 (s, 1H, =CH), 8.11 (d, 2H, *J*= 8.0 Hz), 7.94 (d, 2H, *J*= 4.0 Hz), 1.78 (s, 6H); ^{13}C NMR (400 MHz, $CDCl_3$) δ (ppm): 177.37, 171.90, 147.81, 142.85, 129.18, 126.52, 115.18, 113.13, 112.37, 110.86, 99.43, 99.29, 26.35. All reaction profiles were monitored using thin layer chromatography under UV lamp (254/365 nm). To ensure high purity, the prepared compounds were either re-crystallized or exposed to flash column chromatography (Abou-Yousef et al., 2017; Khattab et al., 2017; Khattab et al., 2016).

2.3. Extraction of cellulose from rice straw

Rice straw used in this study was collected as a waste from Egyptian farms after harvesting in Al-Dakahlia Governorate. Sodium hydroxide, hydrogen peroxide 45% and sulfuric acid (analytical grade) were purchased from Sigma-Aldrich. Rice straw stem was firstly cut into small pieces and thoroughly washed several times using tap water to remove dust and other soluble substances, followed by air drying. The dried rice straw was grinded well with a mill into fine powder. Rice straw powder (100 g) was treated with 10% sodium hydroxide aqueous solution (w/w) with liquor ratio 1:10 for 4 hours at 100°C using mechanical stirrer. This was followed by repeatedly washing process using distilled water till alkali was entirely removed, and finally dried at room temperature. This process was repeated one more time and then further grinded into powder form. The material was then subjected to bleaching using a solution of H_2O_2 (5 g/L; 45% H_2O_2) and sodium silicate (3 g/L). pH was tuned at 10.5 employing an alkaline solution of NaOH. The bleaching process was performed at 95 °C in a liquor ratio of 1:20 for 30 minutes with good stirring. The product was then washed repeatedly using distilled water until the alkali was totally eliminated followed by air-drying. The dried bleached rice straw was grinded well with a mill to afford a fine white cellulose powder (Boonterm et al., 2016). The chemical composition of rice straw was assessed according to standard approaches previously described by Technical Association of Pulp and Paper Industry (TAPPI). Total contents of both cellulose and hemicelluloses were determined using TAPPI/T203/OS/74 standard method; while total content of lignin was determined using TAPPI/T222/OS/83 standard procedure (Boonterm et al., 2016).

2.4. Preparation of cellulose nanowhiskers

The preparation of CNW was carried out according to previously reported literature procedures (Sun et al., 2016). In a three-necked glass flask, the final white cellulose fibers were hydrolyzed with 65 % sulfuric acid, in a liquor ratio of fiber to solution 1:8.75 (w/v) at 45 °C for 15 minutes with vigorous stirring. Then the suspension was diluted with addition of 10 fold distilled water, and exposed to centrifugation at 10000 rpm for 10 minutes. Finally, the resulting nanocellulose gel was filtered and subjected to washing by distilled water to get rid of sulfuric acid. The procedure was repeated three times to eliminate H_2SO_4. The resultant suspension was exposed to dialysis till reaching pH value

of 7. The suspension was then subjected to sonication at 1000 W for 20 minutes in an ice-bath, and finally stored in a refrigerator.

2.5. Fabrication of CNW-TCFH halochromic film

Aqueous solutions of cellulose nanowhiskers (0.5 wt % relative to the volume of water) in a double distilled water was vigorously stirred with sodium alginate (0.5 wt % to the weight of cellulose nanowhiskers), and TCFH solution previously dissolved in lowest amount of acetone (1 mL) at a range of different total contents (0.1, 0.5, 1.5, 2.0 and 2.5 wt % to the total content mass of cellulose nanowhiskers). The solution was then stirred for 24 hours at ambient conditions. The TCFH concentrations, including 0.1, 0.5, 1.5, 2.0 and 2.5 wt % (CNW basis), were denoted as TCFH-1, TCFH-2, TCFH-3, TCFH-4, and TCFH-5, respectively. The final solution was then homogenized at 8000 rpm for 3 minutes by a rotor-stator homogenizer (AD500S-H, Shanghai, China). Urease enzyme (5 mg/ml) was added to the mixture followed by stirring for 30 minutes. Whatman paper samples (2.0 x 5.0 cm) were subjected to dip-coating by padding in the previously prepared aqueous solutions for 10-15 minutes, followed by padding in an aqueous solution of calcium chloride (10 mM) for 10-15 minutes. The Whatman paper strips were then left to dry for 1 hour at ambient conditions.

2.6. Determination of adsorption capacity

The adsorption capacity of TCFH probe molecules onto Whatman paper strips (2.0 x 5.0 cm) were calculated for the prepared solutions (15 mL) at different concentrations of TCFH, including TCFH-1, TCFH-2, TCFH-3, TCFH-4, and TCFH-5, according to the following equation:

$$\text{Adsorption Capacity \%} = \frac{A_0 - A_i}{A_0} \times 100$$

The maximum UV/Vis absorption value (~475 nm) of the prepared solutions at different concentrations of TCFH were recorded before (A_0) and after (A_i) dip-coating the Whatman paper strip into each solution under ambient conditions (25 °C) using UNICAM/UV-visible 300.

2.7. pH measurements of TCFH spectroscopic probe

Methanolic solution of acetic acid (1M) was added to a solution of TCFH to reduce the pH value. The hydrazone anion was generated *in situ* by adding 1M methanolic ammonium hydroxide to solutions of their conjugate acids (TCFH) in acetone.

2.8. Urea sensing experiment

The sensing experiment was carried out at pH= 6.8 using phosphate-EDTA buffer solution (0.1 M) under room temperature and atmospheric pressure. The detection assay was performed according to procedure by Chandler et al (Chandler et al., 1982). Urea was studied in the concentration range of 1-1300 ppm as different solutions were prepared at different concentrations (1, 50, 100, 200, 300, 400, 500, 600, 700, 800, 900, 1000, 1100, 1200 and 1300 ppm). The light yellow colored paper strip biosensor was immersed in each solution for 5-10 minutes at 37^{o}C to develop a pink color due to evolution of ammonia upon the hydrolytic reaction between urea and urease enzyme. The photographs of the paper strips before and after immersion in urea solution were captured by Canon A710-IS digital camera.

2.9. Colorimetric analysis

The coloration analyses of the prepared biosensor at different concentrations of TCFH probe and before and after immersion in urea solution were recorded on Texflash ACS/Data/color 600 spectrophotometer. The coloration parameters were studied by exploring CIE L^* a^* b^* coloration space values, absorption spectra, and color strength (*K/S*), which were recorded using Ultra/Scan/PRO spectrophotometer (Hunter Lab, USA) with an illuminant (D65) and a standard observer (10°). L^* is defined as lightness (dark black (0) to bright white (100)), a^* represents colors in the range of red (+) to green (-), and b^* represents colors in the range of yellow (+) to blue (-).

3. Results and discussion

3.1. Synthesis and photophysical properties of TCFH

The starting material TCF **1** was synthesized according to literature procedure with a yield of 55 % (Khattab et al., 2016). TCFH **4** was simply obtained in high yield of 85 % via azo-coupling reaction between the tricyanofuran coupler **1** and the diazonium chloride salt of 4-formylaniline **2** (Abou-Yousef et al., 2017; Khattab et al., 2017). The azo-coupling reaction occurs in a weak alkaline medium using sodium acetate as a weak base able to deprotonate the active methyl group on the highly electron deficient TCF

moiety. This azo-coupling process generated an unstable azo-based intermediate **3** that was rearranged directly to the stable hydrazone-based molecular structure **4 (Scheme 1)**.

The UV-Vis maximum absorption spectra of TCFH probe **4** were monitored in the range of 443-530 nm **(Table S1 _ supporting information)**. The colors of chromophore **4** in different organic solvents were between orange and purple. Normalized UV-Vis absorption spectra in different solvents are demonstrated in **Figure 1**. A distinct solvatochromic behavior in protic and non-protic solvents was monitored. Protic solvents were able to afford partial protonation of TCFH dye at the lone-pair of electrons on the NH nitrogen atom (Khattab, 2018). This led to reducing the negative charge on the NH nitrogen atom to result in a hypsochromic solvatochromism to shorter wavelength upon increasing solvent polarity. This effect was very small or entirely missing with non-protic solvents. Thus, we had to turn our thought to the dipolar nature of non-protic solvents, by which the solvatochromism could be attributed to the contribution level of lone pair non-bonding electrons on the NH nitrogen atom **(Scheme S1_ supporting information)**. Herein, those lone-pair of electrons can partially proceed as an electron density bridge between the benzaldehyde hydrazone charge donor and TCF heterocyclic charge acceptor in a partial donor-acceptor molecular system. Consequently, this resulted in bathochromic shift upon increasing solvent polarity. Therefore, the polarizability of electron-withdrawing aldehyde group undoubtedly played a major role in promoting solvatochromism.

The electron-withdrawing aldehyde at the *para* site of the arylhydrazone generated an acidic NH proton leading to the creation of benzaldehyde hydrazone conjugate base anion with enhanced electron-donation ability on the hydrazone moiety. The electron-withdrawing aldehyde substituent itself cannot operate as an electron donor. Nonetheless, the hydrazone fragment is able to act as an electron bridge in a push-pull molecular structure or act itself as an electron donor moiety, once conjugating with an electron withdrawing substituent, such as the aldehyde functional group at the *para* position of the arylhydrazone moiety **(Scheme 2)**. This benzaldehyde hydrazone-anion can function as

electron donor in conjugation with the tricyanofuran electron acceptor to result in potentially attractive spectral switching characteristics. **Figure 2** shows the reversible UV-Vis absorption spectra and color shifts of TCFH **4** in acetone (*ca.* 1.7 x 10^{-5} mol L^{-1}) under acid-base conditions as a result of deprotonation/protonation reversible process. When adding tetrabutylammonium hydroxide base in methanol (1.0 mol L^{-1}) to the acetone solution of TCFH probe **4**, the absorption band at 475 nm was subjected to a bathochromic shift to longer wavelength leading to the generation of new absorption band at 530 nm. On the other hand, when adding methanolic trifluoroacetic acid solution (1.0 mol L^{-1}), the absorption band at 475 nm was reappeared (Reichardt, 1994).

To inspect the reversibility of TCFH **4**, 1.0 mol L^{-1} of trifluoroacetic acid and tetrabutylammonium hydroxide in methanol were employed to exchange the pH value back and forth from ~6.55 to ~7.15. The UV-Vis absorption intensity at 475 nm (~0.55) and at 530 nm (~0.67) was recorded as displayed in **Figure 3**. This procedure had a high reversibility proving that TCFH probe **4** had a high stability under acid-base reversible conditions.

3.2. Isolation of cellulose nanowhiskers from rice straw

Pure cellulose is successfully obtained from rice straw via extraction in alkali solution twice to remove wax, hemicellulose, lignin, silica and other soluble components followed by oxidative bleaching process to remove the residual lignin and the white color of the fibers is obtained. This result attributed to both the delignification (breaking the lingo-cellulosic complex) and solubilizing process of hemicellulose which occurs in the alkali treatment process. Furthermore, the bleaching process increased the accessibility of cellulose to promote acidic hydrolysis, resulting in the formation of cellulose nanowhiskers suspension. The chemical composition of the pure cellulose was measured three times and the mean average was presented as follow: 80 % α-cellulose, 0.38 % Kalson lignin, 11.42 % hemicellulose and 8.2 % ash content (Boonterm et al., 2016).

Pure cellulose derived from rice straw is generally fibrous in irregular tens of micrometers or bigger sized archtechtures. As the non-cellulosic contents were detached by dissolution, cellulosic fibers were connected by generating new hydrogen bonding in the drying procedure. Pure cellulose is then sulfuric acid hydrolyzed (8.75 mL/g, 65 wt % H_2SO_4, 45˚C) into cellulose nanowhiskers (CNW). The length of hydrolysis time is 30-45 minutes. Sulfuric acid was diffused and attacking the amorphous cellulosic polymer chains leading to chain degradation into smaller soluble oligosaccharides and sugars, affording cellulose nanocrystals. Additionally, sulfuric acid results in surface esterification to afford cellulose sulfate on the surface of the produced cellulose nanowhiskers, leading to the generation of negatively charged surface to result in repulsive forces preventing CNW from agglomeration in an aqueous suspension (Sun et al., 2016).

3.3. Preparation of CNW-TCFH composite films

Nanomaterials are distinguished by high porous structure, large surface area and excellent surface functionalization (Jayakumar, Menon, Manzoor, Nair, & Tamura, 2010; Khattab, Aly, & Klapötke, 2018; Royston, Ghosh, Kofinas, Harris, & Culver, 2008). Therefore, nanocellulose colorimetric sensor can be considered as an attractive solid-state device for real time detection of a trace target analyte. Compared to a colorimetric probe-based solution, solid state detectors are usually portable, operationally simple, practical, easy to fabricate, fast detector, and inexpensive, making them good candidates in basic laboratory assays as portable detection tools for household and commercial purposes. Thus, the search for an environmentally benign solid state biosensor is of great significance. To a mixture of cellulose nanowhiskers and sodium alginate in distilled water, a solution of tricyanofuran hydrazone in acetone was added. The mixture was stirred for 24 hours at ambient conditions, and homogenized for 3 minutes. The TCFH was added at different concentrations, including 0.1, 0.5, 1.5, 2.0 and 2.5wt% (CNW basis), which denoted as TCFH-1, TCFH-2, TCFH-3, TCFH-4, and TCFH-5, respectively. Urease enzyme was added to the mixture and stirred for thirty minutes. Whatman paper strips were padded in the aqueous solutions of CNW-TCFH, then padded in an aqueous solution of calcium chloride, and finally left to dry for 1 hour under atmospheric conditions. The paper strip detection tool was maintained stable in a

refrigerator for ~5 days without defects. Cellulose nanowhiskers had a major advantage as they improved both porosity and surface area-to-volume ratio of the adsorbing surface. Whatman paper itself consists of micro-scale cellulose fibers, while cellulose nanowhiskers are in the nano-scale. This increased the surface area-to-volume ratio affording a surface with a higher adsorption capacity, and consequently a higher sensitivity to urea analyte. In addition, cellulose nanowhiskers as nano-scale architecture increased the porosity of the exposed surface facilitating the diffusion of urea analyte into the sensor bulk leading to a higher sensitivity (Hoeng et al., 2016; Serpa et al., 2016). The successful immobilization of urease into CNW-TCFH film was primary verified by the visual color shift from light yellow to pink when exposed to ammonia vapor. The adsorption efficiency of the tricyanofuran hydrazone probe onto Whatman paper strips (2.0 x 5.0 cm) were estimated for each solution (15 mL). The prepared solutions, TCFH-1, TCFH-2, TCFH-3, TCFH-4 and TCFH-5, showed adsorption capacities of 62.5, 59.8, 55.1, 48.9 and 41.7, respectively. Thus, a relatively high adsorption capacity was detected at low concentration values of the tricyanofuran hydrazone probe, which can be assigned to the good diffusion of the tricyanofuran hydrazone molecules onto the bulk of the Whatman paper strip owing to the small and planar TCFH molecular structure. Nonetheless, the adsorption capacity decreased upon increasing the total content of the tricyanofuran hydrazone due to reaching the equilibrium of dye uptake onto the paper strip (Georgiadou, Tsatsaroni, Eleftheriadis, & Kehayoglou, 2002; Ujhelyiova, Bolhova, Oravkinova, Tiňo, & Marcinčin, 2007).

3.4. Morphological properties of CNW-TCFH

In general, three dimensional membranes assembled from CNW display high surface area, good porous bulk, and interconnectivity. Those characteristics lead to promising applications in highly sensitive and miniaturized solid state sensors. Both transmission electron microscopy (TEM) and scanning electronic microscope (SEM) were employed to inspect the morphological properties of CNW and CNW-TCFH as shown in **Figure 4**. Sulfuric acid hydrolysis of cellulose results in the breakdown of fibers into rod-like nanocrystals. The amorphous phases were selectively hydrolyzed while the crystalline counterparts remained unaffected (Sun et al., 2016). The CNW with a diameter range of 178-214 nm generated a nonwoven mat of high porosity. The inclusion of TCFH did not

influence the morphological properties of the cellulosic nanowhiskers. It was found that CNW-TCFH nonwoven network displays a light yellow color shifting to pink upon exposure to ammonia released from the reaction of urea with urease enzyme.

The solid state sensor showed high sensitivity to NH_3 liberated from urea/urease reaction. Both large surface to volume ratio and high porosity architecture of the CNW-TCFH biosensor facilitated the dispersion of the diffused guest urea molecules within the sensor matrix to reach the TCFH detection active sites. The elemental content of the dip-coated paper test strip at TCFH concentration (1.5 wt %) was explored by energy-dispersive X-ray spectroscopy (EDS) as demonstrated in **Figure 4e**. The weight percent values for the recognized elements, including carbon, oxygen, chlorine and calcium were monitored at 44.01, 48.29, 4.63 and 3.07, respectively. The energy-dispersive X-ray spectroscopy has been considered for identification of elements at low error. However, as expected, no signals were monitored by EDS for nitrogen atoms which are already shown in the molecular structure of tricyanofuran hydrazone spectroscopic probe. This can be assigned to the very low total content of the tricyanofuran hydrazone probe within the cellulose nanowhiskers.

Fourier-transform infrared FTIR spectra **(Figure 5)** were employed to gain information about chemical structure of CNW and CNW-TCFH. FTIR technique are characterized by the use of small sample size, fast analysis time, operational simplicity, and non-destructive. Considerable increase in the absorption band intensity at 3419 cm^{-1} (hydroxyl stretching) was monitored, which could be assigned to the generated calcium carboxylate $[(COO^-)_2\,Ca^{++}]$ group on alginate polymer chains. Similarly, considerable increment in the absorption band intensity was also monitored at 2907 and 1052 cm^{-1} due to both CH aliphatic stretching and bending, respectively. Additionally, the CH aliphatic stretch was found to shift from 2907 cm^{-1} for CNW to 2964 cm^{-1} for CNW-TCFH. This can be attributed to the extra CH aliphatic groups added from alginate polymer chains. The absorption band at 1447 cm^{-1} belongs to $–CH_2$ symmetrical bending vibration, which disappeared in presence of alginate (CNW-TCFH). The absorption bands at 1024 and 996 cm^{-1} were due to in-plane C–H deformation and C–H deformation vibrations,

respectively. Also, those bands at 1024 and 996 cm^{-1} for CNW were found to shift to 1173 and 1058 cm^{-1} for CNW-TCFH, respectively. The band monitored at 1633 cm^{-1} was attributed to H-O-H bending of water in CNW. However, this band was found to increase in CNW-TCFH due to alginate carbonyl (C=O) group. Thus, FTIR spectra displayed significant shifts in CNW-TCFH absorption bands compared to CNW. This indicated that alginate had significant interactions with CNW matrix. However, no changes in the absorption bands were detected in IR spectra of CNW-TCFH upon increasing the total content of TCFH probe as a result of the very low concentration of TCFH probe loaded on cellulose nanowhiskers. This also confirmed that both TCFH and urease are merely entrapped in the matrix. Similarly, no changes were detected in IR spectra of CNW-TCFH either before or after exposure to the aqueous solutions of urea because of the very low concentration of monitored urea (even at high concentration; 1300ppm).

3.5. Halochromic performance of CNW-TCFH sensory strip

The concentration of the tricyanofuran hydrazone probe and urease enzyme incorporated onto cellulose nanowhiskers was determined in the preparation step. The absorption wavelengths were found to be well-matched with the instant color shifts of the sensor-based nanowhiskers loaded on paper test dipstick. The color shift was monitored by naked-eye to change from light yellow to pink. The colorimetric measurements method has been known as an easy-to-use process. The sensor efficiency was studied by exploring the variations in the CIE (L^*, a^*, b^*) parameters, absorption spectrum and color strength (*K/S*). The total content of tricyanofuran hydrazone as an active sensing component loaded on the nanowhiskers played an important role in functioning the sensory device. The coloration measurements and sensing efficiency at different total contents of tricyanofuran hydrazone are displayed in **Table 1**. After soaking the paper test strips into urea aqueous environment for 10 minutes, the UV-visible absorption spectra were measured. Before and after soaking of the coated paper strips in the urea aqueous solution, a high increment in color strength was monitored indicating a shift to an improved tinctorial strength upon increasing the total content of tricyanofuran hydrazone from 0.1 to 1.5 wt %. A very little shift in the *K/S* value was monitored when increasing tricyanofuran hydrazone total content from 1.5 to 2.5 wt %. The results demonstrated that the optimum colorimetric data were monitored at 1.5 wt % of

tricyanofuran hydrazone. Contacting with urea resulted in an increment in the absorbance wavelength of the paper test strip from 480 to 515 nm.

The colorimetric parameters (L^*, a^* and b^*) of the paper strip at different total content values of tricyanofuran hydrazone were measured before and after exposing to an aqueous medium of urea. The blank paper strip has an off-white color with high L^* (93.21), low b^* (1.34) and low a^* (-0.04). Compared to the blank strip, all treated paper test strip samples showed significantly different values of CIE color coordinates (L^*, a^*, b^*) depending on the concentration of tricyanofuran hydrazone. Before and after dip-coating, L^* was highly reduced demonstrating darker hue upon increasing the total content value of tricyanofuran hydrazone from 0.1 to 1.5 wt %, which can be attributed to the higher uptake of the tricyanofuran hydrazone dye. On the contrary, L^* displayed a negligible change upon raising the total content value of tricyanofuran hydrazone from 1.5 to 2.5 wt % owing to the reduced uptake of the tricyanofuran hydrazone dye. L^* displayed a considerable change after exposing to the urea aqueous solution as shown by the darker shade produced at the tricyanofuran hydrazone dye concentrations of 1.5, 2.0 and 2.5 wt %. Before subjecting to urea, the increased a^* and b^* positive values showed changes in the hue of the sensor paper test strips from off-white for untreated sample to light yellow for treated samples upon raising the tricyanofuran hydrazone concentration from 0.1 to 2.5 wt %. After exposing to urea, the increased negative b^* and positive a^* magnitudes were translated to pink. After dip-coating, the sensor paper strips displayed color shift from light yellow to pink within 5-10 minutes, during which the urea/urease reaction generated ammonium ions to change the urea aqueous medium pH to higher value.

The paper dipstick sensory system was successfully used to approximate an unknown concentration value of CO $(NH_2)_{2(aq)}$ depending on an assembled a calibration curve (1-1300 ppm) as demonstrated in **Figure 6** and **Table S2 (**supporting information). After exposure to urea, the absorption intensity of the paper dipstick at 515nm exhibited a linear curve upon increasing urea concentration. Visual color change was detected upon raising urea concentration due to generation of ammonia which in turn abstract proton

from the hydrazone NH. The identification limit of the paper test dipstick for urea was determined by measuring its absorbance changes to recognize the first absorbance intensity value at 0.09 (515 nm) for the urea concentration at 50 ppm. After raising urea concentration to 1100 ppm, no further increments in the absorption intensity (1.393; 515 nm) were monitored. The wavelength of the absorption maxima was found to shift from 480 to 515 nm. The dipstick paper sensor was retained stable in refrigerator for ~5 days. **Figure 6** shows the calibration curve for the detection of urea employing paper strip detector dip-coated with CNW/urease enzyme/tricyanofuran hydrazone. The process depends on the shifts of the absorption intensity of the sensor paper test strip at 515 nm after detection of urea in an aqueous environment and upon increasing the total content of urea from 50 to 1100 ppm.

3.6. Dipstick detection mechanism

pH responsiveness of TCFH was established by integrating an aldehyde-bearing phenylhydrazone fragment acting as an electron-donating moiety upon deprotonating the hydrazone NH to generate hydrazone anion bearing negative charge. The strongly active electron-withdrawing aldehyde substituent at the *para*-position of the phenylhydrazone afforded a highly acidic NH hydrazone. This highly electron-withdrawing aldehyde substituent resulted in an enhancement in the stability of the formed hydrazone anion to generate a push-pull molecular system with an extended conjugation and consequently with different color depending on the degree of conjugation **(Figure 7)**. Degradation of urea into ammonia can be driven by urease catalytic reaction. Increasing urea concentration led to clear pH change to higher values as a result of an enzymatic catalytic hydrolysis reaction of urea leading to generation of alkaline ammonia on the surface of the TCFH/Urease-activated nanowhiskers, which consequently transform color from light yellow to pink. The generated ammonia cannot be bonded to the carboxylate anions on alginates which are not free as they are already bonded via cross-linking to calcium ions (Rehan et al., 2019). Thus, the urease motivated hydrolysis of urea ($CO(NH_2)_2$) into ammonia can be translated into a visual readout color shift owing to a deprotonation procedure of tricyanofuran-hydrazone spectroscopic probe by the generated alkaline ammonia.

4. Conclusion

TCFH and urease enzyme were introduced into the alginate/CNW matrix to produce a pH-film sensor. Combination between TCFH, alginate biomolecules and CNW afforded a composite film comprising different coloration measurements depending on TCFH concentration. We presented a biosensor tool merging the urease enzyme catalytic performance toward urea analyte to allow monitoring this enzymatic catalytic activity in presence of pH sensitive tricyanofuran hydrazone spectroscopic active sites. The urease reaction was explored by monitoring the colorimetric shifts due to increasing the pH of the urea solution path as a result of the urea conversion into ammonia. The current approach can be applied to determine the urea concentration in biological fluids, such as urine and blood. The colorimetric measurements verified that the biosensor exhibited a detection limit in the range of 50-1100 ppm. The visual color change of TCFH probe dissolved in acetone solution varied from light yellow to pink in the pH range of 6.55-7.15, while the resulting film responded well to ammonia released from urea/urease reaction in an aqueous environment. The film could be utilized as a naked-eye sensing label or test strip as the color shift of the film introduce a simple and practical technique to monitor urea. The dipstick sensor demonstrated a very good sensitivity. Due to their efficiency and simplicity, such urea detector tool can be used to monitor and indicate urea in the stored foodstuff and other urea-containing products.

Author Contribution Statement

Tawfik A. Khattab: Extraction of cellulose from rice straw, Dipstick detection mechanism, writing, reviewing and editing. **Moustafa M. G. Fouda:** Writing original draft. **Mohamed Rehan:** Morphological properties of CNW-TCFH, writing, reviewing and editing. **Mohammad K. Okla:** Fabrication of CNW-TCFH halochromic film. **Saudi A. Alamri:** Urea sensing experiment and halochromic performance of CNW-TCFH sensory strip. **Ibrahim A. Alaraidh:** Preparation of cellulose nanowhiskers and determination of adsorption capacity. **Abdullah A. AL-ghamdi:** Colorimetric analysis. **Walid H. Soufan:** Synthesis and photophysical properties of TCFH. **Eslam M. Abdelsalam:** Determination of adsorption capacity, reviewing and editing. **Ahmed A. Allam:** Writing original draft.

Acknowledgements

We extend our appreciation to the Dean of Scientific Research, King Saud University, for funding the work through the research group project number PRG-1439-63. The authors also thank the Deanship of Scientific Research and RSSU at King Saud University for their technical support. Technical support from National Research Centre, Cairo, Egypt; is also gratefully acknowledged.

References

Abou-Yousef, H., Khattab, T. A., Youssef, Y. A., Al-Balakocy, N., & Kamel, S. (2017). Novel cellulose-based halochromic test strips for naked-eye detection of alkaline vapors and analytes. *Talanta,* 170, 137-145.

Boonterm, M., Sunyadeth, S., Dedpakdee, S., Athichalinthorn, P., Patcharaphun, S., Mungkung, R., & Techapiesancharoenkij, R. (2016). Characterization and comparison of cellulose fiber extraction from rice straw by chemical treatment and thermal steam explosion. *Journal of Cleaner Production,* 134, 592-599.

Cai, W., Xie, S., Zhang, J., Tang, D., & Tang, Y. (2018). Immobilized-free miniaturized electrochemical sensing system for Pb2+ detection based on dual Pb2+-DNAzyme assistant feedback amplification strategy. *Biosensors and Bioelectronics,* 117, 312-318.

Carter, K. P., Young, A. M., & Palmer, A. E. (2014). Fluorescent sensors for measuring metal ions in living systems. *Chemical reviews,* 114(8), 4564-4601.

Chandler, H., Cox, J., Healey, K., MacGregor, A., Premier, R., & Hurrell, J. (1982). An investigation of the use of urease-antibody conjugates in enzyme immunoassays. *Journal of immunological methods,* 53(2), 187-194.

Coresh, J., Astor, B. C., Greene, T., Eknoyan, G., & Levey, A. S. (2003). Prevalence of chronic kidney disease and decreased kidney function in the adult US population: Third National Health and Nutrition Examination Survey. *American journal of kidney diseases,* 41(1), 1-12.

Cruys-Bagger, N., Ren, G., Tatsumi, H., Baumann, M. J., Spodsberg, N., Andersen, H. D., . . . Westh, P. (2012). An amperometric enzyme biosensor for real-time measurements of cellobiohydrolase activity on insoluble cellulose. *Biotechnology and bioengineering,* 109(12), 3199-3204.

D'Apolito, M., Du, X., Pisanelli, D., Pettoello-Mantovani, M., Campanozzi, A., Giacco, F., . . . Giardino, I. (2015). Urea-induced ROS cause endothelial dysfunction in chronic renal failure. *Atherosclerosis,* 239(2), 393-400.

Desai, R. M., Koshy, S. T., Hilderbrand, S. A., Mooney, D. J., & Joshi, N. S. (2015). Versatile click alginate hydrogels crosslinked via tetrazine–norbornene chemistry. *Biomaterials,* 50, 30-37.

Dong, J. X., Gao, Z. F., Zhang, Y., Li, B. L., Zhang, W., Lei, J. L., . . . Luo, H. Q. (2016). The pH-switchable agglomeration and dispersion behavior of fluorescent Ag nanoclusters and its applications in urea and glucose biosensing. *NPG Asia Materials,* 8(12), e335.

Duong, H. D., & Rhee, J. I. (2015). Development of a ratiometric fluorescent urea biosensor based on the urease immobilized onto the oxazine 170 perchlorate-ethyl cellulose membrane. *Talanta,* 134, 333-339.

Fan, X., White, I. M., Shopova, S. I., Zhu, H., Suter, J. D., & Sun, Y. (2008). Sensitive optical biosensors for unlabeled targets: A review. *analytica chimica acta,* 620(1-2), 8-26.

Georgiadou, K., Tsatsaroni, E., Eleftheriadis, I., & Kehayoglou, A. (2002). Disperse dyeing of polyester fibers: kinetic and equilibrium study. *Journal of applied polymer science,* 85(1), 123-128.

Grishkewich, N., Mohammed, N., Tang, J., & Tam, K. C. (2017). Recent advances in the application of cellulose nanocrystals. *Current Opinion in Colloid & Interface Science*, 29, 32-45.

Hoeng, F., Denneulin, A., & Bras, J. (2016). Use of nanocellulose in printed electronics: a review. *Nanoscale*, 8(27), 13131-13154.

Jayakumar, R., Menon, D., Manzoor, K., Nair, S., & Tamura, H. (2010). Biomedical applications of chitin and chitosan based nanomaterials—A short review. *Carbohydrate polymers*, 82(2), 227-232.

Jha, V., Garcia-Garcia, G., Iseki, K., Li, Z., Naicker, S., Plattner, B., . . . Yang, C.-W. (2013). Chronic kidney disease: global dimension and perspectives. *The lancet*, 382(9888), 260-272.

Kharitonov, A. B., Zayats, M., Lichtenstein, A., Katz, E., & Willner, I. (2000). Enzyme monolayer-functionalized field-effect transistors for biosensor applications. *Sensors and Actuators B: Chemical*, 70(1-3), 222-231.

Khattab, T. A. (2018). Novel solvatochromic and halochromic sulfahydrazone molecular switch. *Journal of Molecular Structure*, 1169, 96-102.

Khattab, T. A., Aly, S. A., & Klapötke, T. M. (2018). Naked-eye facile colorimetric detection of alkylphenols using Fe (III)-impregnated silica-based strips. *Chemical Papers*, 72(6), 1553-1559.

Khattab, T. A., Dacrory, S., Abou-Yousef, H., & Kamel, S. (2019a). Development of microporous cellulose-based smart xerogel reversible sensor via freeze drying for naked-eye detection of ammonia gas. *Carbohydrate polymers*, 210, 196-203.

Khattab, T. A., Dacrory, S., Abou-Yousef, H., & Kamel, S. (2019b). Smart microfibrillated cellulose as swab sponge-like aerogel for real-time colorimetric naked-eye sweat monitoring. *Talanta*, 205, 120166.

Khattab, T. A., Fouda, M. M., Abdelrahman, M. S., Othman, S. I., Bin-Jumah, M., Alqaraawi, M. A., . . . Allam, A. A. (2019). Co-encapsulation of enzyme and tricyanofuran hydrazone into alginate microcapsules incorporated onto cotton fabric as a biosensor for colorimetric recognition of urea. *Reactive and Functional Polymers*, 142, 199-206.

Khattab, T. A., Fouda, M. M., Allam, A. A., Othman, S. I., Bin-Jumah, M., Al-Harbi, H. M., & Rehan, M. (2018). Selective Colorimetric Detection of Fe (III) Using Metallochromic Tannin-Impregnated Silica Strips. *ChemistrySelect*, 3(43), 12065-12071.

Khattab, T. A., Kassem, N. F., Adel, A. M., & Kamel, S. (2019). Optical Recognition of Ammonia and Amine Vapor Using "Turn-on" Fluorescent Chitosan Nanoparticles Imprinted on Cellulose Strips. *Journal of fluorescence*, 1-10.

Khattab, T. A., Rehan, M., Aly, S. A., Hamouda, T., Haggag, K. M., & Klapötke, T. M. (2017). Fabrication of PAN-TCF-hydrazone nanofibers by solution blowing spinning technique: Naked-eye colorimetric sensor. *Journal of environmental chemical engineering*, 5(3), 2515-2523.

Khattab, T. A., Tiu, B. D. B., Adas, S., Bunge, S. D., & Advincula, R. C. (2016). Solvatochromic, thermochromic and pH-sensory DCDHF-hydrazone molecular switch: response to alkaline analytes. *RSC Advances*, 6(104), 102296-102305.

Kim, J.-H., Shim, B. S., Kim, H. S., Lee, Y.-J., Min, S.-K., Jang, D., . . . Kim, J. (2015). Review of nanocellulose for sustainable future materials. *International Journal of Precision Engineering and Manufacturing-Green Technology*, 2(2), 197-213.

Kumari, S., Chauhan, G. S., Ahn, J.-H., & Reddy, N. (2016). Bio-waste derived dialdehyde cellulose ethers as supports for α-chymotrypsin immobilization. *International journal of biological macromolecules*, 85, 227-237.

Kunduru, K. R., Basu, A., Abtew, E., Tsach, T., & Domb, A. J. (2017). Polymeric sensors containing P-dimethylaminocinnamaldehyde: Colorimetric detection of urea nitrate. *Sensors and Actuators B: Chemical*, 238, 387-391.

Kunduru, K. R., Kutcherlapati, S. R., Arunbabu, D., & Jana, T. (2017). *Armored Urease: Enzyme-Bioconjugated Poly (acrylamide) Hydrogel as a Storage and Sensing Platform*. In *Methods in enzymology* (pp. 143-167): Elsevier

Länge, K., Rapp, B. E., & Rapp, M. (2008). Surface acoustic wave biosensors: a review. *Analytical and bioanalytical chemistry*, 391(5), 1509-1519.

Levey, A. S., Eckardt, K.-U., Tsukamoto, Y., Levin, A., Coresh, J., Rossert, J., . . . Eknoyan, G. (2005). Definition and classification of chronic kidney disease: a position statement from Kidney Disease: Improving Global Outcomes (KDIGO). *Kidney international*, 67(6), 2089-2100.

Lin, N., Gèze, A., Wouessidjewe, D., Huang, J., & Dufresne, A. (2016). Biocompatible double-membrane hydrogels from cationic cellulose nanocrystals and anionic alginate as complexing drugs codelivery. *ACS applied materials & interfaces*, 8(11), 6880-6889.

Liu, J., & Lu, Y. (2006). Fast colorimetric sensing of adenosine and cocaine based on a general sensor design involving aptamers and nanoparticles. *Angewandte Chemie International Edition*, 45(1), 90-94.

Liu, Y.-L., Liu, R., Qin, Y., Qiu, Q.-F., Chen, Z., Cheng, S.-B., & Huang, W.-H. (2018). Flexible electrochemical urea sensor based on surface molecularly imprinted nanotubes for detection of human sweat. *Analytical chemistry*, 90(21), 13081-13087.

Meng, Z., Stolz, R. M., Mendecki, L., & Mirica, K. A. (2019). Electrically-transduced chemical sensors based on two-dimensional nanomaterials. *Chemical reviews*, 119(1), 478-598.

Palmas, F., Mussap, M., & Fattuoni, C. (2018). Urine metabolome analysis by gas chromatography–mass spectrometry (GC–MS): Standardization and optimization of protocols for urea removal and short-term sample storage. *Clinica Chimica Acta*, 485, 236-242.

Palomo, V., Díaz, S. A., Stewart, M. H., Susumu, K., Medintz, I. L., & Dawson, P. E. (2016). 3, 4-dihydroxyphenylalanine peptides as nonperturbative quantum dot sensors of aminopeptidase. *ACS nano*, 10(6), 6090-6099.

Penner, R. M. (2017). A nose for hydrogen gas: fast, sensitive H2 sensors using electrodeposited nanomaterials. *Accounts of chemical research*, 50(8), 1902-1910.

Rabinovich, M. L., Vasil'chenko, L. G., Karapetyan, K. N., Shumakovich, G. P., Yershevich, O. P., Ludwig, R., . . . Yaropolov, A. I. (2007). Application of cellulose-based self-assembled tri-enzyme system in a pseudo-reagent-less biosensor for biogenic catecholamine detection. *Biotechnology Journal: Healthcare Nutrition Technology*, 2(5), 546-558.

Rehan, M. F., Farid, O., Ibrahim, S., Hassan, A. A., Abdelrazek, A., Khafaga, N., & Khattab, T. A. (2019). Green and sustainable encapsulation of Guava leaf extracts (Psidium Guajava L.) into alginate/starch microcapsules for multifunctional finish over cotton gauze. *ACS Sustainable Chemistry & Engineering*.

Reichardt, C. (1994). Solvatochromic dyes as solvent polarity indicators. *Chemical reviews*, 94(8), 2319-2358.

Royston, E., Ghosh, A., Kofinas, P., Harris, M. T., & Culver, J. N. (2008). Self-assembly of virus-structured high surface area nanomaterials and their application as battery electrodes. *Langmuir*, 24(3), 906-912.

Schoolaert, E., Hoogenboom, R., & De Clerck, K. (2017). Colorimetric nanofibers as optical sensors. *Advanced Functional Materials*, 27(38), 1702646.

Serpa, A., Velásquez-Cock, J., Gañán, P., Castro, C., Vélez, L., & Zuluaga, R. (2016). Vegetable nanocellulose in food science: A review. *Food Hydrocolloids*, 57, 178-186.

Sha, R., Komori, K., & Badhulika, S. (2017). Graphene–Polyaniline composite based ultra-sensitive electrochemical sensor for non-enzymatic detection of urea. *Electrochimica Acta*, 233, 44-51.

Shao, Y., Wang, J., Wu, H., Liu, J., Aksay, I. A., & Lin, Y. (2010). Graphene based electrochemical sensors and biosensors: a review. *Electroanalysis: An International Journal Devoted to Fundamental and Practical Aspects of Electroanalysis*, 22(10), 1027-1036.

Stoytcheva, M., Zlatev, R., Cosnier, S., Arredondo, M., & Valdez, B. (2013). High sensitive trypsin activity evaluation applying a nanostructured QCM-sensor. *Biosensors and Bioelectronics*, 41, 862-866.

Su, X., Jiang, H., & Wang, X. (2015). Thiols-induced rapid photoluminescent enhancement of glutathione-capped gold nanoparticles for intracellular thiols imaging applications. *Analytical chemistry*, 87(20), 10230-10236.

Sun, B., Zhang, M., Hou, Q., Liu, R., Wu, T., & Si, C. (2016). Further characterization of cellulose nanocrystal (CNC) preparation from sulfuric acid hydrolysis of cotton fibers. *Cellulose*, 23(1), 439-450.

Testani, J. M., Cappola, T. P., Brensinger, C. M., Shannon, R. P., & Kimmel, S. E. (2011). Interaction between loop diuretic-associated mortality and blood urea nitrogen concentration in chronic heart failure. *Journal of the American College of Cardiology*, 58(4), 375-382.

Ujhelyiova, A., Bolhova, E., Oravkinova, J., Tiňo, R., & Marcinčin, A. (2007). Kinetics of dyeing process of blend polypropylene/polyester fibres with disperse dye. *Dyes and Pigments*, 72(2), 212-216.

Valeur, B., & Leray, I. (2000). Design principles of fluorescent molecular sensors for cation recognition. *Coordination Chemistry Reviews*, 205(1), 3-40.

Virgen-Ortíz, J. J., dos Santos, J. C., Berenguer-Murcia, Á., Barbosa, O., Rodrigues, R. C., & Fernandez-Lafuente, R. (2017). Polyethylenimine: a very useful ionic polymer in the design of immobilized enzyme biocatalysts. *Journal of Materials Chemistry B*, 5(36), 7461-7490.

Wang, J. (2005). Carbon-nanotube based electrochemical biosensors: A review. *Electroanalysis: An International Journal Devoted to Fundamental and Practical Aspects of Electroanalysis*, 17(1), 7-14.

Webster, A. C., Nagler, E. V., Morton, R. L., & Masson, P. (2017). Chronic kidney disease. *The lancet*, 389(10075), 1238-1252.

Zaccheo, B. A., & Crooks, R. M. (2011). Self-powered sensor for naked-eye detection of serum trypsin. *Analytical chemistry*, 83(4), 1185-1188.

Zhang, M., Lin, H., Shen, L., Liao, B.-Q., Wu, X., & Li, R. (2017). Effect of calcium ions on fouling properties of alginate solution and its mechanisms. *Journal of membrane science*, 525, 320-329.

Zhang, R., & Chen, W. (2017). Recent advances in graphene-based nanomaterials for fabricating electrochemical hydrogen peroxide sensors. *Biosensors and Bioelectronics*, 89, 249-268.

Zheng, M., Xie, Z., Qu, D., Li, D., Du, P., Jing, X., & Sun, Z. (2013). On–off–on fluorescent carbon dot nanosensor for recognition of chromium (VI) and ascorbic acid based on the inner filter effect. *ACS applied materials & interfaces*, 5(24), 13242-13247.

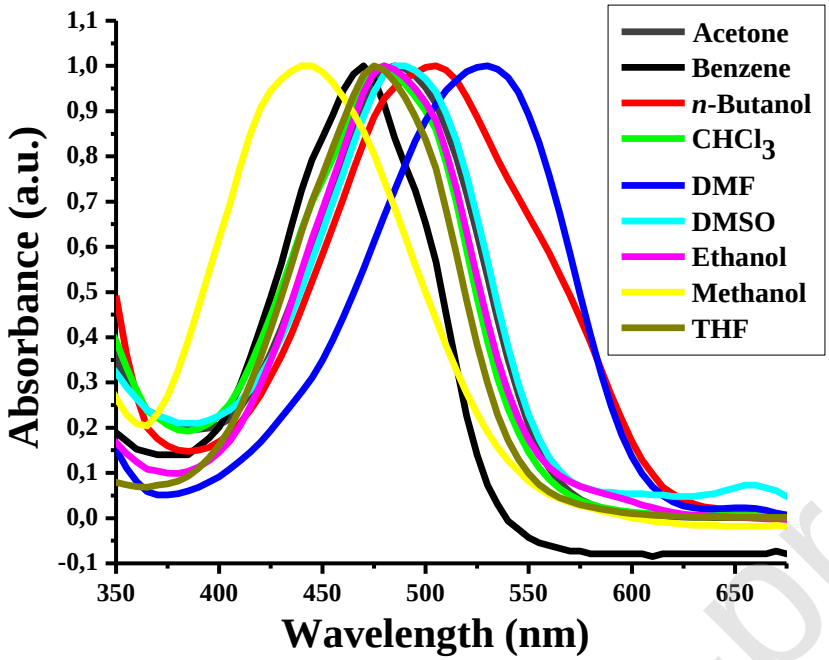

Figure 1: Normalized UV-Vis absorption spectra of the tricyanofuran hydrazone spectroscopic probe **4** in some selected solvents

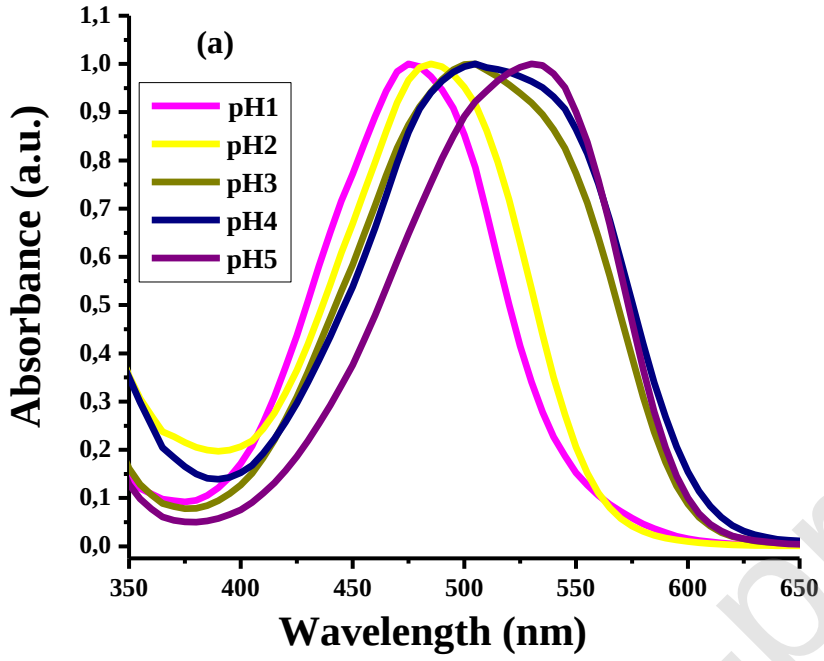

Figure 2: (a) pH correlated UV-Vis absorption spectra, and (b) color shift from orange, red to purple upon changing pH between 6.55 (Orange; pH1 at 475 nm), 6.75 (pH2 at 485 nm), 6.95 (Red; pH3 at 505 nm), 7.05 (pH4 at 505 nm), and 7.15 (Purple; pH5 at 530 nm) respectively; of TCFH **4** in acetone solution (*ca*. 1.7 x 10^{-5} mol L^{-1})

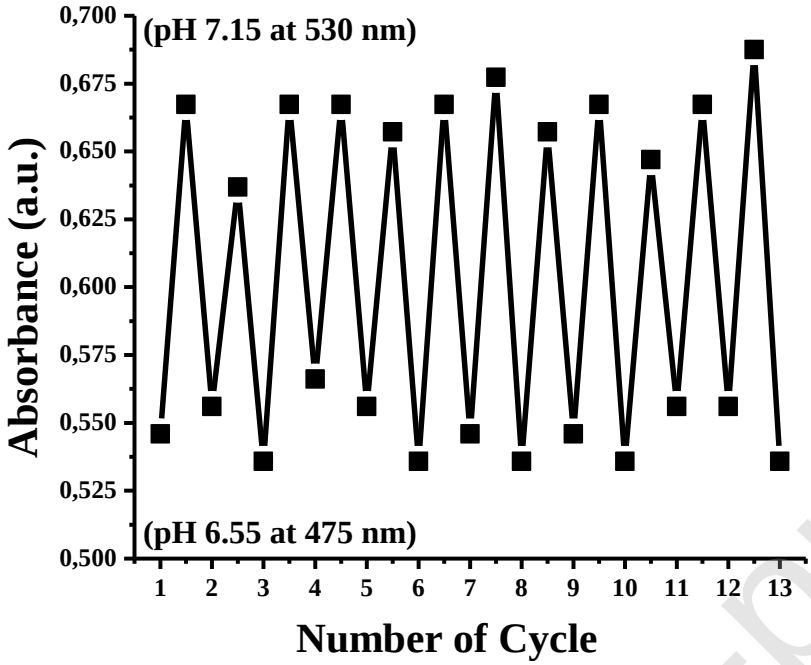

Figure 3: Ratio of absorption intensity at 475 and 530 nm of TCFH **4** in acetone (*ca.* 1.7 x 10^{-5} mol L^{-1}) upon changing pH from 6.55 to 7.15

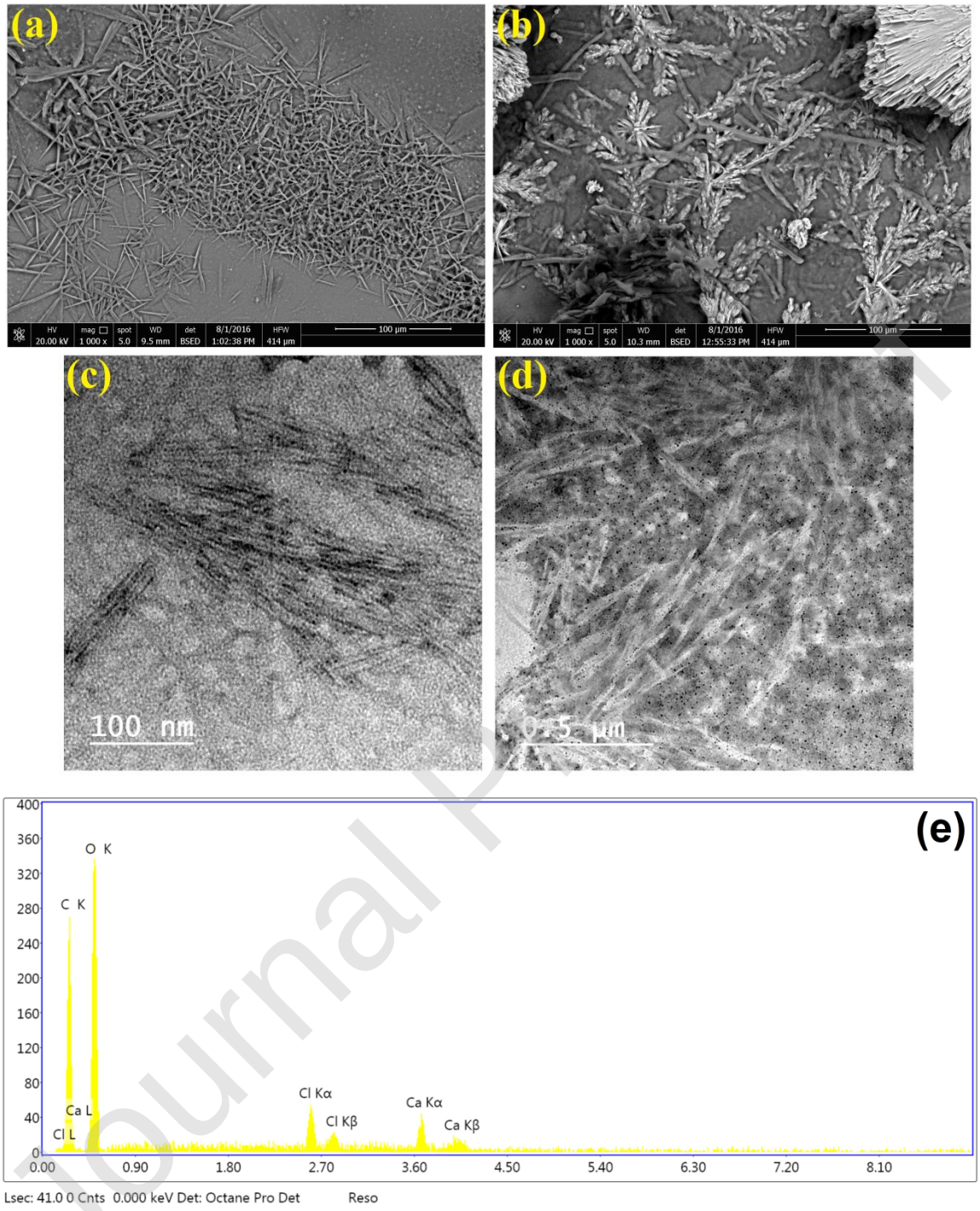

Figure 4: SEM (*top*) and TEM (*bottom*) images of CNW (a, c) and CNW-TCFH (b, d); TCFH Conc. 1.5 wt % and elemental content diagram of the paper dipstick assay (TCFH Conc. 1.5 wt %) (e)

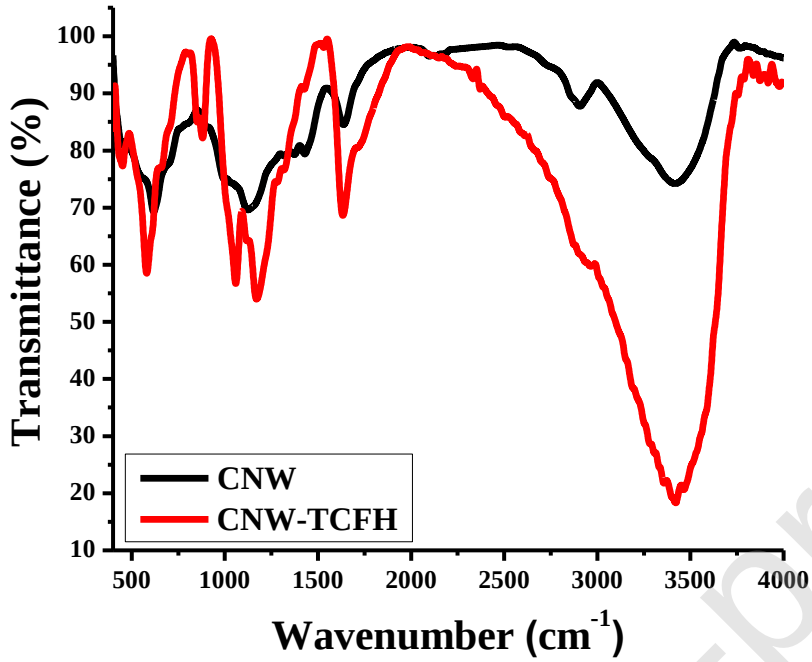

Figure 5: FTIR spectra of both CNW and CNW-TCF (TCFH Conc. 1.5 wt %)

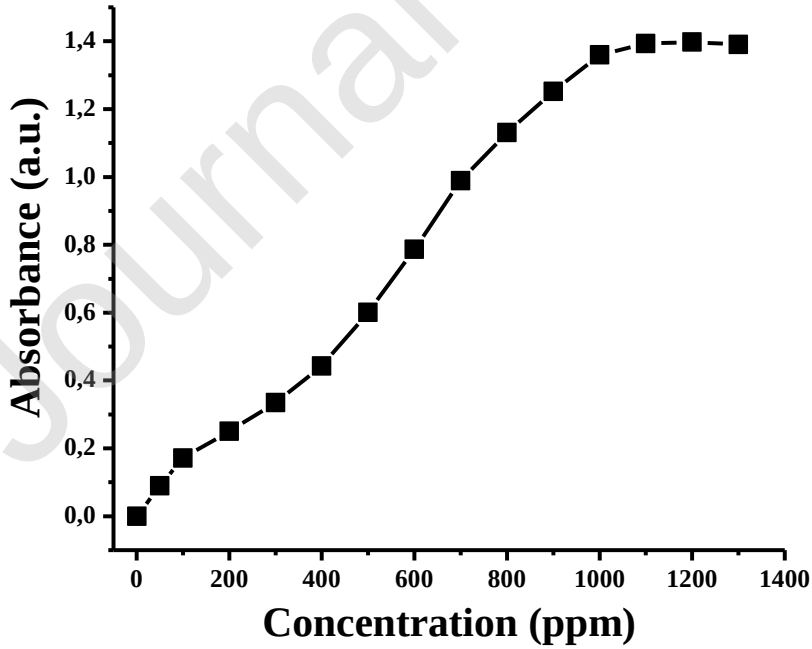

Figure 6: Absorption maxima of treated paper test strip at 515nm as a result of urea sensory when raising the aqueous urea concentration from 1 to 1300 ppm

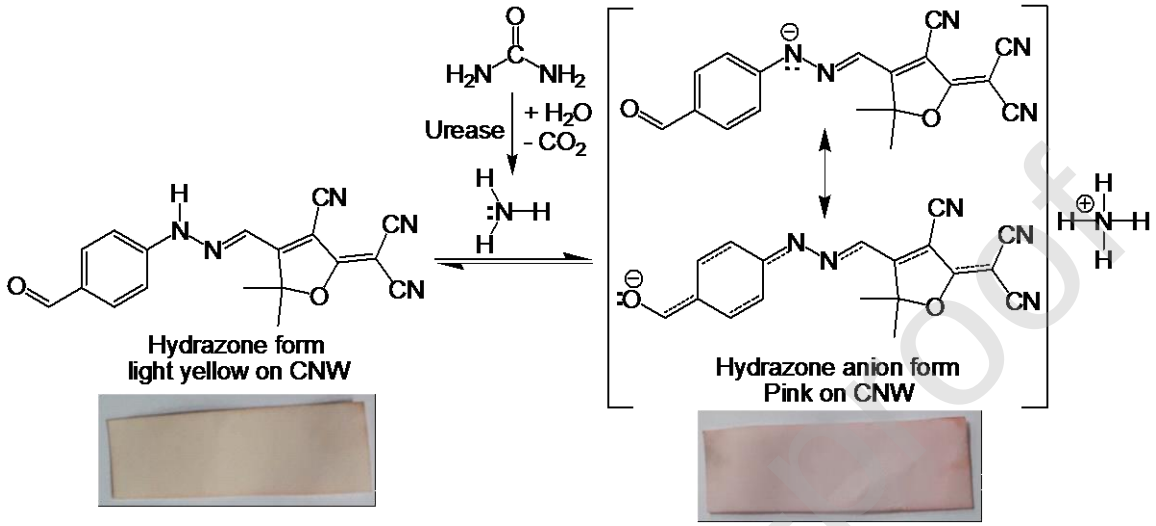

Figure 7: Suggested mechanism of tricyanofuran hydrazone probe for colorimetric detection of urea demonstrating color shift of treated paper test strip from light yellow to pink

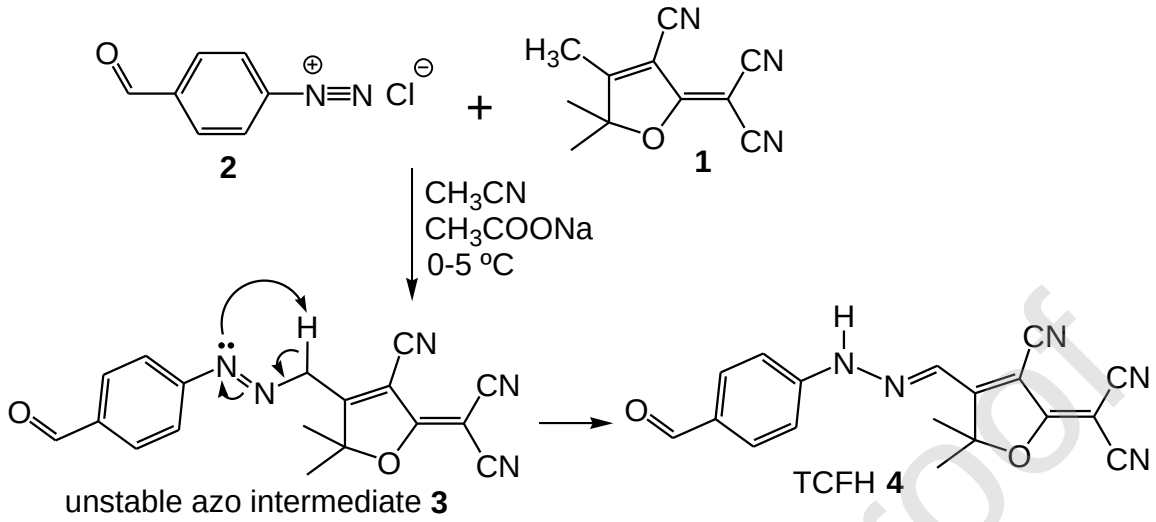

Scheme 1: Synthesis of TCFH chromophore **4**

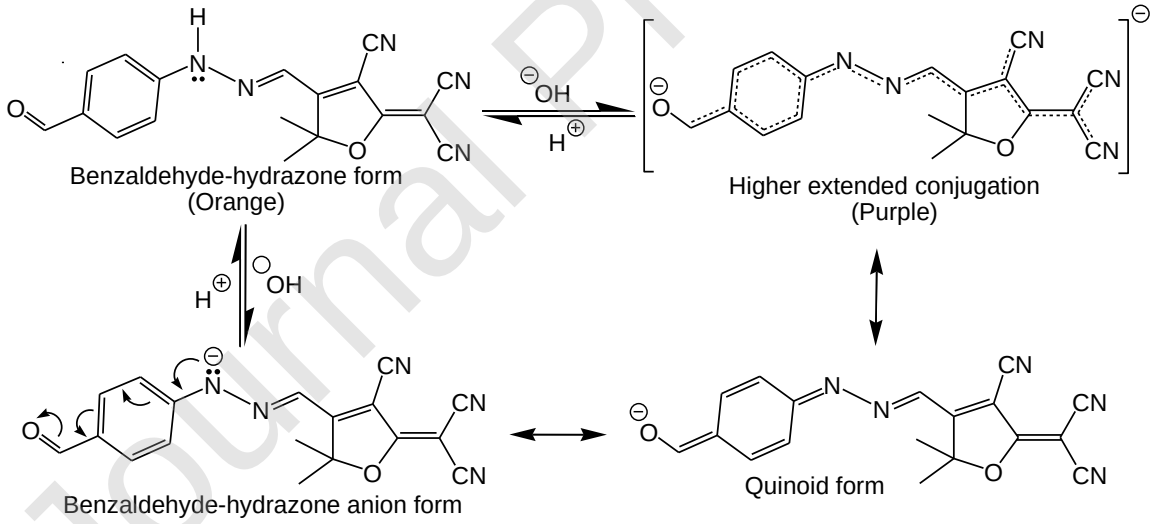

Scheme 2: Molecular switching mechanism of tricyanofuran hydrazone **4** probe consisting of Push (benzaldehyde hydrazone-anion) and Pull (tricyanofuran heterocycle) system

Table 1: Colorimetric screening of coated paper strips at different total content of tricyanofuran hydrazone before and after sensing the ammonia liberated from a recently prepared aqueous urea solution (Conc. 1100 ppm).

TCFH	**L***		**a***		**b***		***K/S***	
(wt %)	**before**	**after**	**before**	**after**	**before**	**after**	**before**	**after**
0.1	**73.75**	**60.01**	**3.38**	**5.54**	**11.49**	**-3.92**	**3.15**	**3.82**
0.5	**70.33**	**56.60**	**5.01**	**8.19**	**15.06**	**-4.15**	**4.97**	**5.47**
1.5	**63.09**	**43.59**	**8.66**	**10.22**	**22.66**	**-8.95**	**8.19**	**7.47**
2.0	**62.50**	**43.90**	**8.30**	**12.36**	**22.83**	**-9.09**	**8.01**	**9.40**
2.5	**61.82**	**42.27**	**9.28**	**15.52**	**27.81**	**-12.29**	**8.82**	**9.76**